Unraveling the Intricacies of Surface Salt Formation on Mg(0001): Implications for Chloride-Ion Batteries

Kanchan Sarkar,[1] Darius Hübner,[1] Daniel Stottmeister,[1] and Axel Groß[1,2]

[1] *Institute of Theoretical Chemistry, Ulm University, 89069 Ulm, Germany*
[2] *Helmholtz Institute Ulm (HIU), Electrochemical Energy Storage, 89081 Ulm, Germany*

We present a density functional theory study of the initial steps of chlorine deposition on the Mg(0001) surface. Such processes occur in chloride-ion batteries in which lithium and magnesium are used as anode materials. In addition, it is also of fundamental interest, as halide adsorption on metal electrodes is an important process in interfacial electrochemistry. We discuss the adsorption properties and determine the stable adsorption structures, both with respect to the free chlorine molecule but also as a function of the electrode potential. We find indications of the immediate formation of the $MgCl_2$ surface salt structure upon exposure of Cl to a Mg surface. These findings are discussed with respect to the conversion of the Mg anode to a $MgCl_2$ configuration which provides the thermodynamical driving force for the discharge of a Cl-ion battery.

Keywords: density functional calculations, chloride adsorption, metal electrodes, surface salt formation, chloride-ion batteries, polyhedra similarity measures

INTRODUCTION

The interaction of halides with metal anodes is of general interest in electrochemistry, as halides are typical anions present in electrolytes [1–3]. Understanding the interaction between adsorbates and metal surfaces is essential for designing efficient electrode materials for energy storage and conversion applications [4]. Recently the interaction of chloride with lithium and magnesium electrodes has become of interest in the context of chloride ion batteries (CIBs) [5–7] in which lithium and magnesium can be used as the anode material [8]. Batteries based on anions such as chloride represent an alternative to the widely used Li-ion batteries as they are typically based on more abundant materials and also exhibit theoretical energy densities which can be higher than those of current lithium ion batteries [9, 10]. Thus they contribute to more sustainable and environmentally friendly energy storage technologies.

Yet, the interaction of halides with metal surfaces is also interesting from a surface science point of view. It has been known for a long time that the adsorption of halogen atoms on metal surfaces can lead to an anomalous decrease in the work function [11–14]. Typically, one would expect that the adsorption of negatively charged species such as anions on a surface would lead to a dipole moment at the surface that would increase the workfunction of the metal surface. Results of first-principles electronic structure calculations using density functional theory have demonstrated that this anomalous behavior can be attributed to a strong polarization of the halogen atoms upon adsorption [15–17].

To the best of our knowledge, the adsorption of chlorine on magnesium has not been intensively studied yet from a computational point of view. The existing studies were motivated by the fact that chlorine adsorption could lead to the corrosion of Mg metals [18–20]. These computational studies found that Cl preferentially adsorbs in the three-fold hollow positions on Mg(0001) associated with a slight increase in the workfunction. Upon the operation of a Cl-ion batteries, the metal anode will be converted to a chloride salt which provides the thermodynamical driving force for the discharge of a Cl-ion battery. The energy gain upon this conversion does in fact represent the driving force in the Cl-ion battery operation [5, 6]. This means that the adsorption of chlorine on the metal anode does only correspond to the first step in the anode conversion upon discharge. Still, it is interesting from a fundamental as well as from an applied point of view how the overall conversion of the metal anode on Cl-ion batteries from a bulk metal to a chloride salt proceeds.

It is well-known that metals can form so-called surface oxides, i.e. thin adsorbed films with an oxide-like structure, upon the exposure of metals to an oxygen atmosphere as a function of the oxygen concentration [21, 22]. Hence the question arises whether metal surfaces upon the exposure to halogen species might form equivalent structure corresponding to a *surface salt*, i.e., thin films with metal-halide like structures. In fact, the existence of Pb-NO_3 surface salts has been predicted by first-principles calculations for Pb(111) electrodes in the presence of a nitrate electrolyte [23, 24]. These surface salts have been suggested to be instrumental in the functioning of atomic-scale transistors [24–26].

In this computational study, we will consider the adsorption of chlorine on the most stable surface termination of magnesium, Mg(0001) [27] for a range of different coverages by means of density functional theory calculations. Using grand-canonical concepts [28–31], we will

determine the thermodynamically stable chlorine surface structures on Mg(0001) as a function of electrochemical control parameters. Thus we will test whether surface salt structures might be a stable intermediate in the conversion of a Mg anode to $MgCl_2$ upon discharge of a Mg-ion battery.

COMPUTATIONAL DETAILS

We have used the Vienna Ab initio Simulation Package (VASP) [32, 33] to perform periodic density functional theory (DFT) calculations which are well-suited to tackle basic battery-relevant problems [34]. Exchange-correlation effects have been taken into account within the generalized gradient approximation (GGA) employing the functional of Perdew, Burke, and Ernzerhof (PBE) [35], as this functional is well-suited to reproduce the properties of metals [2, 36]. The core electrons are represented by projector augmented wave (PAW) pseudopotentials [37] as supplied in VASP [38]. An energy cutoff of 810 eV has been chosen in the expansion of the wave functions in plane waves in order to safely ensure convergence of the results. Likewise, a $16 \times 16 \times 16$ Monkhorst-Pack $k-$point grid has been used for the bulk metal calculations and $5\times5\times1$ k-points for the eight-layer slab calculations with 3×3 surface unit cells yielding converged results for the integration over the first Brillouin zone. The slabs were separated by 15 Å of vacuum. The electronic tolerance at each ionic step has been chosen to be 10^{-7} eV based on a Gaussian smearing of 0.02 eV width.

Magnesium crystallizes in the hcp structure. The computed equilibrium lattice parameters for bulk hcp-Mg ($a = 3.195$ Å and $c/a = 1.627$) agree well with experimental values of 3.21 Å and 1.62. Likewise, the calculated cohesive energy of -1.52 eV/atom compares nicely with the experimental results (-1.51 eV/atom) [39–41]. Mg(0001) corresponds to a hexagonal close-packed surface. The layers of Mg(0001) are relaxed until the force on every atom is smaller than 0.01 eV/Å to secure convergence. Surface energetics and electronic structures have been explored first using 0.1 eV Methfessel-Paxton smearing followed by a final energy extrapolation to zero broadening.

The high symmetry sites of Mg (0001) correspond to atop, hcp, fcc, and bridge positions (see Fig. 1). As described in detail below, the hollow site (hcp or fcc) is affirmed to be the favored adsorption site over the bridge and on-top positions. The relative stabilities go on as f (fcc) $\sim$ h (hcp) $>$ t (top) $>>$ b (bridge). On-surface atop and bridge positions are meta- and unstable, respectively. Therefore, we focus on fcc, hcp, or both these adsorption

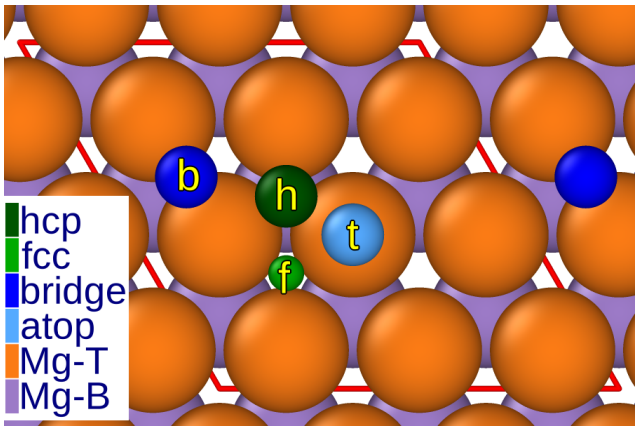

FIG. 1. Different adsorption sites on the Mg (0001) surface, indicating their positions relative to the underlying surface structure. The surface is depicted as a slab, with the top layer represented by Mg-T atoms and the 7 bottom layers represented by Mg-B atoms. The adsorption sites, including hcp (hexagonal close-packed), fcc (face-centered cubic), bridge, and atop, are indicated by small spheres of different colors.

locales alongside top positions with coverages between 0.11 and 2.44 ML. Besides, we perform adsorption calculations over one face by comparing computational outcomes for both the single and double-faced metal slabs.

The adsorption energies $E_{\rm ads}$ per adsorbate of N_{ads} adsorbates within a given unit cell have been calculated according to

$$E_{\rm ads} = \frac{1}{N_{ads}} \left(E_{\rm tot} - (E_{\rm surf} + N_{ads} E_{\rm a})\right) \ , \qquad (1)$$

where $E_{\rm surf}$ and $E_{\rm a}$ are the total energies of the clean surface and the adsorbate in its most stable structure, respectively, and $E_{\rm tot}$ is the total energy of the adsorption system. The most stable form of chlorine is the Cl_2 molecule in the gas phase, so that $E_{\rm a}$ correspond to half of the binding energy of the Cl_2 molecule. Note furthermore that with the binding energy of stable adsorbates we denote the absolute value of the adsorption energy, $E_b = |E_{\rm ads}|$.

Note that thermodynamically the stable adsorbate structures are not determined by the adsorption energy per adsorbate, but rather by the adsorption energy per surface area. Furthermore, under equilibrium conditions the energy of the adsorbates is given by the adequate chemical or electrochemical potential. Thus the central

quantity is the free surface energy of adsorption [30]

$$\begin{aligned}\Delta\gamma(T,p) &= \frac{\Delta G_{ads}(T,p)}{A_s} \\ &= \frac{1}{A_s}\left(G_{ads}(T,p,N_{ads}) - G_{ads}(T,p,0)\right. \\ &\quad \left. -N_{ads}\ \mu_{ads}(T,p)\right) \end{aligned} \tag{2}$$

In electrochemical systems, the electrochemical potential instead of the chemical potential enters the determination of the surface energy of adsorption. In order to obtain convenient expressions for the electrochemical potential, we use the concept of the computational hydrogen electrode (CHE) [29] which can also be applied to the adsorption of halogen atoms such as chlorine using the redox couple $\frac{1}{2}\ \mathrm{Cl_2} + e^- \rightleftarrows \mathrm{Cl^-}$ [42, 43] yielding an electrochemical potential of

$$\begin{aligned}\tilde{\mu}\big(\mathrm{Cl^-(aq)}\big) - \mu(e^-) = \frac{1}{2}\mu\big(\mathrm{Cl_2(g)}\big) + e(U_{\mathrm{SHE}} - U^0) \\ +k_{\mathrm{B}}T\ln a_{\mathrm{Cl^-}}\ .\end{aligned} \tag{3}$$

Here, $U^0 = 1.36$ is the reduction potential of the chloride vs. U_{SHE} [42, 43] and $a_{\mathrm{Cl^-}}$ its activity coefficient. Finally, we replace the free energy G_{ads} appearing in Eq. 2 by the total energy E_{ads} per adsorbate which is often done in applications of the CHE concept and which typically still yields satisfactory results for the adsorption of strongly bound small adsorbates such as hydrogen and chlorine [31]. Thus we obtain the following expression of the free surface energy of adsorption as a function of the electrode potential,

$$\Delta\gamma(U_{\mathrm{SHE}}) = \frac{N_{\mathrm{ads}}}{A_s}\left(E_{\mathrm{ads}} - e(U_{\mathrm{SHE}} - U^0)\right)\ , \tag{4}$$

where we assume standard conditions, which means that the activity of the halides $a_{\mathrm{A^-}}$ is unity. For other concentrations of the halides, the electrode potential needs to be shifted by $k_{\mathrm{B}}T\ln a_{\mathrm{A^-}}$ which corresponds to 59 meV for a change of the activity by one order of magnitude at room temperature.

RESULTS AND DISCUSSION

Interlayer Spacing on Mg(0001) Surface

The behavior of the Mg(0001) surface deviates significantly from conventional metal surfaces, as evidenced by an unconventional expansion in the first interlayer spacing compared to its bulk structure. Typically, the topmost atoms on a metal surface layer form stronger bonds with the underlying layer, leading to a contraction in the interlayer spacing [44, 45]. However, both computational simulations and experimental studies provide compelling evidence supporting an approximate expansion of 1.95% in the first interlayer spacing for the Mg(0001) surface [46–48].

While the behavior of the first interlayer spacing on the Mg(0001) surface has received considerable attention and is thus well-documented [46–48], the second interlayer spacing has sparked debate in the literature. Notably, experimental findings by Sprunger et al. [47] and theoretical estimates [46] (and references therein) indicate an expansion of approximately 0.8%. In contrast, our calculations, complemented by atomic structure analysis employing low-energy electron diffraction (LEED) [48] intensity measurements, reveal a slight reduction of about −0.03%. Although this discrepancy may seem subtle, it underscores the intricate nature of interlayer interactions on the Mg(0001) surface and emphasizes the significance of precision in future investigations. We ensured accuracy and precision in our calculations by employing enhanced computational settings, as outlined in the computational methods section. Additionally, we expanded the system to include 8 layers, as a well-converged interlayer relaxation necessitates at least 7 layers for hcp Mg(0001) surface, analogous to surface energy and work function studies [46]. Regarding the subsequent interlayer spacings, we observed the following changes with respect to the ideal spacing: −0.16% (expt. $0.4 \pm 0.4\%$ [47] and 0.0% [48]), −0.1%, −0.16%, −0.03%, 1.95%.

Cl Adatom Adsorption Preferences and Energetics on the hcp Mg(0001) Surface

As far as the adsorption behavior on hcp metal surfaces is concerned, computational studies consistently demonstrate that typically the most stable adsorption configurations are found at the hollow (hcp and fcc) sites and the bridge site [44, 45], as evidenced by the calculated binding energy (E_b). These sites offer favorable interactions due to the proximity and coordination of the adsorbate with the surface atoms, resulting in a stronger binding. In contrast, the atop site, lacking neighboring metal substrate atoms, exhibits weaker bonding interactions.

For the specific case of Cl adsorption on Mg(0001), we examined the optimal adsorption position for a single Cl adatom within a 3×3 unit cell. Note that adsorption of Cl on the Mg(0001) surface predominantly occurs on the surface rather than filling the subsurface tetra or octasites [49]. Consistent with the observed trend, we found that the hcp site exhibits the most favorable adsorption with an adsorption energy of −2.587 eV, closely followed by the fcc site with an adsorption energy of −2.581 eV. These results indicate a preference for high-coordinated adsorption sites on Mg(0001). Notably, the singly-coordinated top site emerges as the next most favorable adsorption site with an energy of −2.308

eV, while the doubly-coordinated bridge site corresponds to an unstable local maximum. Cl binding to Mg(0001) is thus by about 0.6 eV stronger than to Cu(111), but considerably weaker by about 1.4 eV than Cl adsorption on Ca(111) and Sr(111) [17, 43]. Note furthermore that the energy gain upon Cl adsorption on Mg(0001) is larger than upon $MgCl_2$ formation which is about -1.5 eV per formula unit depending on the particular $MgCl_2$ bulk structure. This means that thermodynamically first the formation of a Cl adsorbate layer on Mg(0001) is stable, and only for higher Cl exposures or higher electrode potentials the formation of $MgCl_2$ bulk becomes feasible.

Cl structures on Mg(0001) at higher coverages

In the following, we consider higher chlorine surface coverages within the 3×3 surface unit cell. Our primary focus remains on the hcp and fcc positions for Cl adsorption on the Mg(0001) surface, given their higher demonstrated adsorption stability. With respect to the adsorption of chlorine on metal surfaces such as Pt(111) and Cu(111), it is well-known that there is a repulsive dipole-dipole interaction between the adsorbates [43] which favors adsorption structures with the largest mutual distance between the adsorbates. The adsorption energies per Cl atom as a function of coverage at the fcc and hcp sites are plotted in the inset of Fig. 2. Except for the coverage 2/3, Cl adsorption at the fcc sites is more stable. Overall the decrease in the binding energies due to the mutual repulsion of the adsorbed Cl atoms is well visible.

Interestingly enough, for a chlorine coverage of 2/9, we find the structure with the two chlorine atoms at adjacent fcc hollow sites with a Cl–Cl distance of 3.5 Å more stable than the structure with a larger mutual distance exceeding 5.2 Å (see Fig. 3a and b). Furthermore, the binding energy per Cl atom at a coverage of 1/3 in a hexagonally close-packed structure (Fig. 3d) is even stronger than at a coverage of 1/9. Such a trend in the Cl adsorption for the 1/3 coverage of halogen atoms has been found before, in particular for Cl/Pt(111) [43]. This has been explained by the fact that this arrangement does not only correspond to a two-dimensional close-packed structure but it is at the same time the arrangement with the largest mutual distances among the adsorbates for a given coverage. Still, it is interesting to note that this behavior is particularly strong for chlorine adsorption on Mg(0001) which might be explained by the larger lattice constant of Mg compared to those of late transition metals which allows the Cl atom to adsorb closer to the surface so that the mutual repulsion is even further reduced.

The free surface energies of adsorption plotted in Fig. 2 yield at the same time a surface phase diagram of the most stable surface adsorbate structures as a function of the electrode potential. At electrode potentials above $U = -1.27$ V, chlorine adsorption sets in with a coverage of 1/3 which will then be replaced at higher electrode potentials by the structure with a coverage of 4/9. A similar behavior as a function of electrode potential has also been obtained for Cl adsorption on Cu(111) and Pt(111) [43].

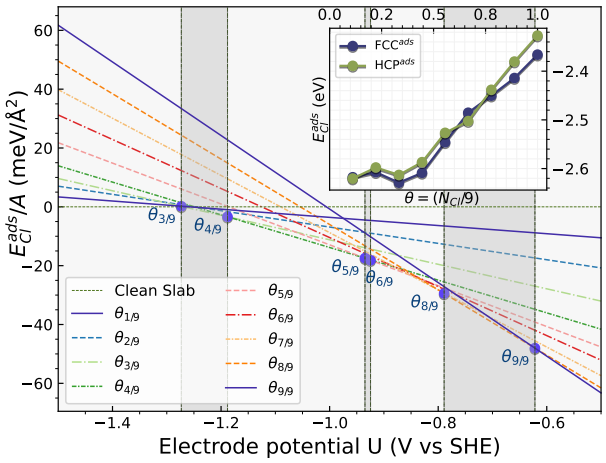

FIG. 2. Free surface energies of adsorption for chlorine adsorption structures as a function of the electrode potential for surface coverages between 1/9 and 1. The stable structures are given by lowest surface energies as a function of the electrode potential. The inset shows the adsorption energy per Cl atom as a function of coverage for adsorption at the fcc and hcp sites.

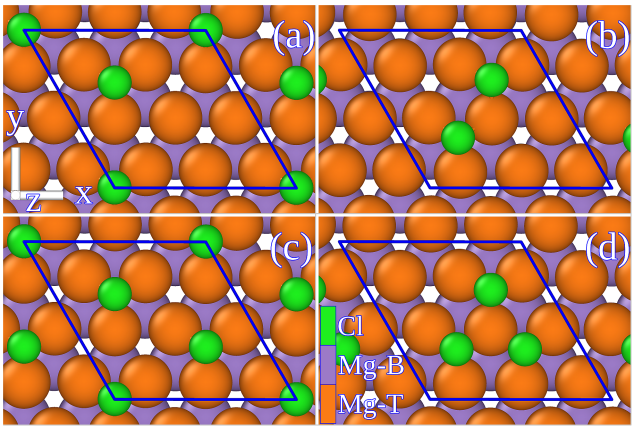

FIG. 3. Structural arrangement of Cl adsorption sites at Cl coverages of 2/9 (panels a and b) and 1/3 (panels c and d).

Influence of higher chlorine coverage on the Mg(0001) surface

The adsorption behavior of chlorine on the Mg(0001) surface takes an intriguing turn when additional Cl atoms are introduced after reaching full monolayer coverage ($\Theta = 1.0$). We have been looking for the onset of the formation of a $MgCl_2$ layer on Mg(0001) by using an efficient yet computationally inexpensive optimization algorithm called adaptive random mutation hill climbing (ARMHC) [50–52].

Efforts to engineer minimal energy adsorption structures have predominantly been build around manually crafted initial structural designs, followed by optimization through established techniques rooted in solid-state physics, such as empirical, semi-empirical, or DFT calculations. While effective for lower adsorbate coverages, this conventional approach grapples with the challenge of accommodating higher adsorbate loads. However, a promising avenue lies in the application of Evolutionary Computing (EC) techniques, as demonstrated by Sarkar *et al.* and their referenced works [50]. In essence, EC approaches encompass a spectrum of optimization strategies inspired by the mechanisms of natural selection and genetic inheritance. These methods exhibit computational intelligence and inherent adaptability, enabling them to swiftly identify critical regions within the solution space [51].

The employed ARMHC algorithm commences with one initial educated guess and then iteratively refines the positions of the Cl atoms and Mg atoms of the top two surface layers by minimizing the energy determined by VASP single point calculations with low computational setups. The approach leverages mutation as its sole evolutionary process, with two adjustable parameters – mutation probability and mutation intensity – dynamically fine-tuned based on continuous performance evaluation. This strategy involves the random exploration of superior solutions within the vicinity of the current solution by introducing controlled mutations into the adsorption structure. Consequently, ARMHC represents a thoughtfully devised methodology for rapidly generating initial trial solutions in the quest for optimal adsorption structures. For in-depth details, please refer to the code provided in the referenced work [52]. Several plausible initial geometries, tailored to specific adsorbate coverages, have been crafted using the ARMHC algorithm. These geometries are then subjected to rigorous relaxation studies using the VASP code.

By adopting this strategy, we efficiently explored the extensive configuration space and successfully identified stable and energetically favorable arrangements of Cl atoms on the Mg(0001) surface at nominally high coverages, including $\Theta = 10/9, 11/9, 4/3, 13/9,$ and 2.0. This comprehensive investigation allowed us to uncover previously unknown equilibrium structures and gain deeper insights into the adsorption behavior of Cl on the Mg(0001) surface and stability under electrochemical conditions.

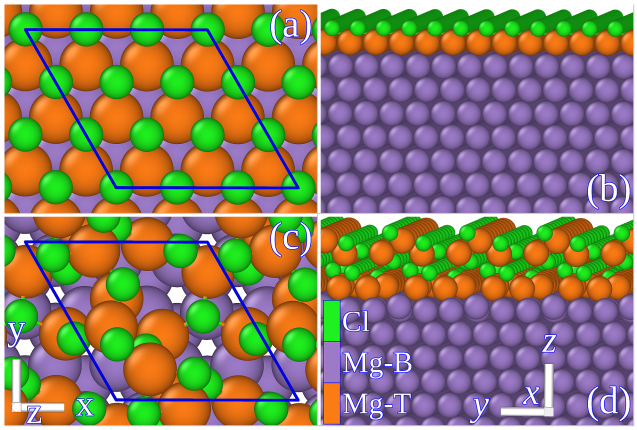

FIG. 4. Top and site views of Cl adsorbate structures at a complete Cl monolayer coverage ($\Theta = 1$) (panels a and b) and at a coverage of $\Theta = 10/9$ (panels c and d). The surface Mg atoms (Mg-T) are shown in orange, while the lower seven Mg layers (Mg-B) are represented in violet. The Cl atoms are displayed in green. The introduction of an additional Cl atom on the (3×3) surface unit cell disrupts the flat adsorption pattern and leads to a much more open surface structure.

In contrast to lower coverages, where simpler adsorption structures tend to dominate, the range of energetically favorable structures becomes notably diverse at $1 < \Theta \leq 2$. Accommodating additional Cl atoms on the surface initiates complex adsorption processes, leading to significant reconfiguration of the Mg(0001) surface. Variations in the behavior of surface Mg atoms, involving both elevating and relocating in response to Cl adsorption, result in a multifaceted energy landscape within this coverage range. Numerous local minima with subtle energy differences characterize this landscape, demanding a comprehensive exploration of structural possibilities and their energy landscapes for stability determination. We therefore employed ARMHC algorithms with a variety of wide-ranging initial geometries to fully exploit and explore the complex potential landscapes for each studied coverages in the range of $1 < \Theta \leq 2$.

As the chlorine coverage on the Mg(0001) surface approaches and surpasses a monolayer ($\Theta = 1.0$), a notable transition in the surface structure becomes apparent. Fig. 4 illustrates this transition through energy minimum structures at nominal Cl coverage of 1 (panels a, b) and 10/9 (panels c, d). In the formation of the $\Theta = 10/9$ structure (panel c or d), a distinct reconstruction of the Mg surface occurs. Here, Cl atoms,

along with the top-layer surface Mg atoms from $\Theta = 1.0$ (panel a or b), undergo a shift and elevation into the Cl layer and beyond with the introduction of an additional Cl atom. This transition, as the Cl coverage surpasses $\Theta = 1.0$, is characterized by a sudden shift in stability, as evidenced by a significant alteration in the binding energy of -0.23 eV per adsorbed Cl atom. The inset of Fig. 5 illustrates this discontinuity, providing a clear and compelling illustration of the evolving adsorption behavior. It is important to note that the extent and nature of surface reconstructions in the vicinity of the Cl adsorbate layer exhibit a lack of a consistent patterns and instead display significant variation across the $1 < \Theta \leq 2$ coverage range. These variations are a consequence of the intricate interplay between Cl-Mg and Cl-Cl interactions, which become increasingly pronounced with the inclusion of extra Cl atoms. Therefore, the intuitive introduction of additional Cl atom(s) to the $\Theta = 10/9$ minimum energy structure does not necessarily lead to a predictable transition to the $\Theta = 11/9$ minimum energy structure or subsequent states. This makes it challenging to foresee specific structural outcomes. However, it is worth mentioning that all the identified energy minimum structures at coverages $1 < \Theta \leq 2$ exhibit no Cl-Cl bonding, even when considering a minimum Cl-Cl distance of 3.25 Å for potential bond formation. This observation is in line with experimentally observed trigonal $MgCl_2$ salt structures ($P3\overline{m}1$ and $R\overline{3}m$ [53, 54]), which feature a Cl-Cl distance of approximately 3.04 Å. The observations underscore the dynamic nature of the Cl-Mg(0001) system when exposed to higher chloride concentrations, where the interaction between Cl atoms is primarily governed by their interactions with the surface and the surrounding metal atoms, rather than the formation of Cl-Cl bonds.

The adsorption energies and free surface energies of adsorption as a function of the electrode potential for chlorine coverages $0 < \theta \leq 2$ are plotted in Fig. 5. It becomes obvious that $\Theta = 2.0$ is associated with the largest binding energy per chlorine atom among the considered structures (see the inset of Fig. 5). Considering the $\theta = 2$ structure in the plot of the free surface energies of adsorption, it turns out to exhibit a maximum binding energy per Cl atom leading to the lowest onset potential in the phase diagram In addition, the largest coverage among the considered structures in Fig. 5 leads to a steeper slope of the free surface energies. Thus this structure becomes thermodynamically more stable than all other energetically stable structures with lower coverages. Therefore, upon exposure of the Mg(0001) electrode to chloride at sufficiently high electrode potentials, a salt-like surface structure can be immediately formed as a precursor for the conversion of the Mg electrode to a $MgCl_2$ crystal.

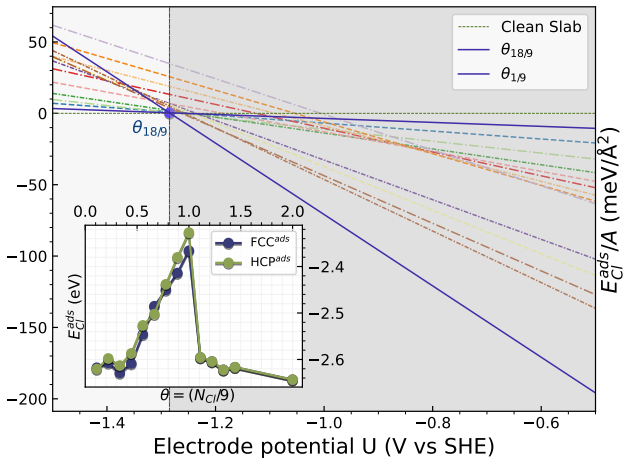

FIG. 5. Free surface energies of adsorption for chlorine adsorption structures as a function of the electrode potential for surface coverages between 1/9 and 2. The stable structures are given by lowest surface energies as a function of the electrode potential. The inset shows the adsorption energy per Cl atom as a function of coverage for adsorption at the fcc and hcp sites on which the free surface energies are based.

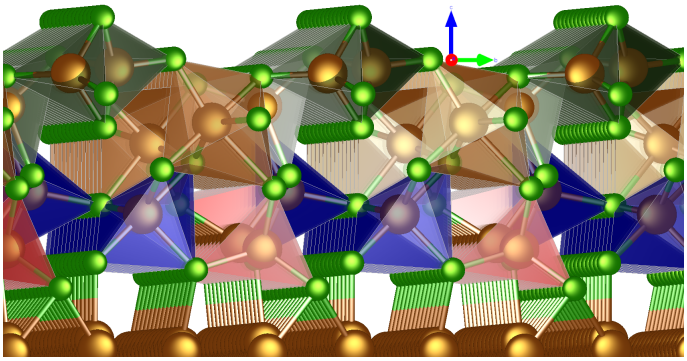

FIG. 6. Illustration of the most stable Cl adsorbate structure for a nominal Cl coverage of $\Theta_{Cl} = 2$ on Mg(0001).

Analysis of the formed surface salt structures

We will now present an analysis of the structure of the surface salt formed with a nominal coverage of 2 (see Fig. 6). To understand the different polyhedra present in this adsorption configuration, we examined the Mg-Cl coordinated distances in all $MgCl_2$ salt structures, which ranged from 2.35 Å for fourfold-coordinated configurations to a maximum of 2.67 Å for sixfold-coordinated configurations. The remarkable feature of the MgCl layer structure lies in the diverse coordination environments adopted by the top layer Mg atoms, with each being surrounded by 3 to 6 Cl atoms. By employing Voronoi polyhedra analysis, we quantified the local coordination en-

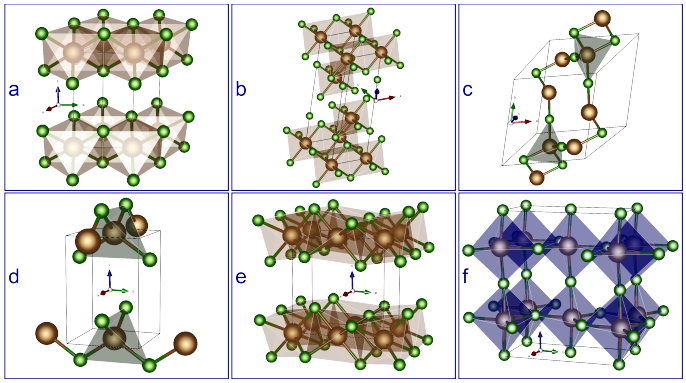

FIG. 7. Illustration of different (meta-)stable $MgCl_2$ salt structures [55]. hexa coordinated: a, b, e, penta coordinated: f, tetra coordinated: c, d. The a, b $MgCl_2$ salt structures have been found experimentally whereas structures c-f correspond to numerically found meta-stable structures.

vironment of each Mg atom and determined the number of shared faces with neighboring atoms in the adsorption structure. To account for lattice mismatch effects, a slightly higher (8.6 % compared to the maximum 2.67 Å Mg-Cl distance) coordination distance of 2.9 Å for Mg-Cl was adopted. Our analysis revealed that 22.2% of Mg atoms were threefold-coordinated (with Mg-Cl bond distances between 2.43$\mathring{A}$ and 2.69 Å), 33.3% were fourfold-coordinated (with Mg-Cl bond distances between 2.3$\mathring{A}$ and 2.45 Å), 22.2% were fivefold-coordinated (with Mg-Cl bond distances between 2.35$\mathring{A}$ and 2.67 Å), and 22.2% were sixfold-coordinated (with Mg-Cl bond distances between 2.43$\mathring{A}$ and 2.9 Å).

Indeed, the $\Theta = 2.0$ structure (Fig. 6) does not correspond to a layer of any of the energetically possible $MgCl_2$ modifications (Fig. 7(a) to (f)) due to the incompatibility arises from the lattice mismatch between the Mg(0001) substrate and the possible layer configurations. For the very similar reasson, at the juncture where the metal slab meets the salt-like structures, the Mg atoms exhibit a tri-coordinated arrangement, in contrast to the 4 to 6 coordinated Mg atoms characteristic of all known $MgCl_2$ salt structures. Nonetheless, as we move to elevated levels along the z axis, we do observe coordination environments that bear similarities to reported salt structures.

To assess the local coordination environments within the adsorption structures, we employed several robust goodness measures to compare polyhedral similarities for matching polyhedra of each top layer Mg atoms with reference salt structures. However, as none of them was sufficient to fully capture the complexities of structural similarity or dissimilarity between polyhedra, we leveraged local structure descriptors, specifically the radial

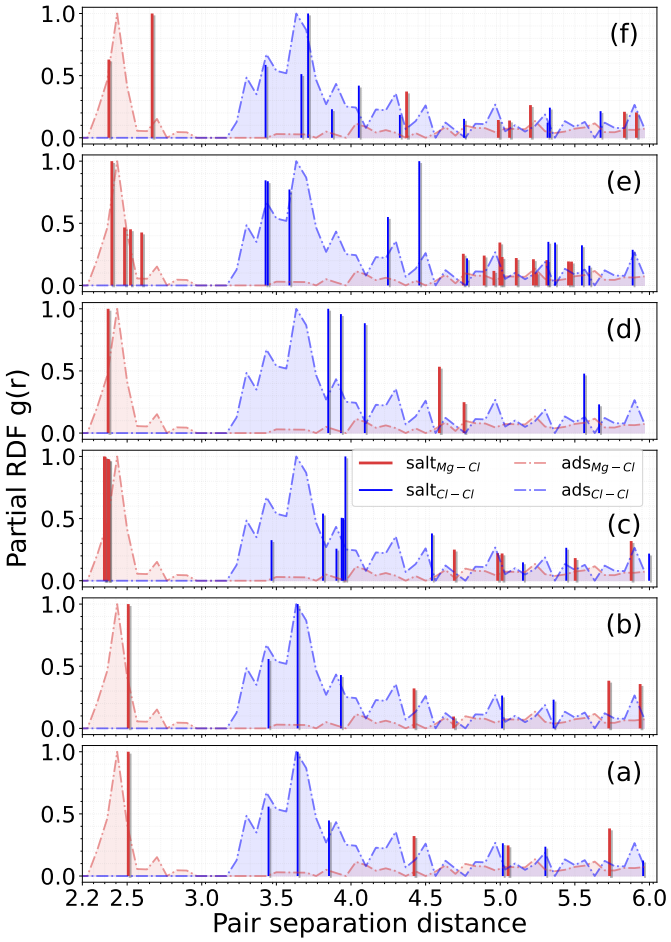

FIG. 8. Comparison of the radial distribution functions for Mg-Cl (red) and Cl-Cl (blue) distances. Dash-dotted lines: RDFs for the most stable Cl/Mg(0001) structure at a coverage of $\Theta_{HF_{2.0}}$, plotted in the background with a broadening. Bars: RDFs of the $MgCl_2$ salt structures depicted in Fig. 7(a) to (f). (a) experimental trigonal omega ($P3\overline{m}1$), (b) experimental trigonal omega ($R\overline{3}m$), (c) triclinic ($\overline{P}1$) (d) tetragonal ($\overline{P}4m2$) (e) orthorhombic Pmma (f) orthorhombic Ama2.

pair distribution function (RDF), for the intuitive local perspective on the atomic arrangement around each atom [56]. The radial pair distribution function $g_{\alpha\beta}(r)$ quantifies the likelihood of finding a particle β at a distance r from a reference particle α, with α positioned at $r = 0$. Essentially, it creates a histogram of pairwise particle distances. In our case, involving two particle species, Mg and Cl, $g(r)$ yields three distinct partial functions: $g_{MgMg}(r)$, $g_{MgCl}(r)$, and $g_{ClCl}(r)$. We corroborate our findings by presenting a visual representation in Fig. 8, where we plot the normalized partial RDFs $g_{MgCl}(r)$ and $g_{ClCl}(r)$ of the adsorbate structure in the background, with normalized partial RDFs of experimental and theoretical $MgCl_2$ salt structures as foreground

overlays. Here, "normalized" refers to scaling with respect to the maximum value of that particular partial RDF.

In Fig. 8 *a* and *b*, the juxtaposition showcases the seamless amalgamation of all foreground peaks within the background RDF. First of all, it is obvious that no RDF of one particular $MgCl_2$ bulk structure matches the RDF of the Cl adsorbate structure. However, all of the considered $MgCl_2$ bulk structures at least partially coincide with the surface salt structure. There is a particular good agreement between the surface salt structure and the experimentally observed trigonal omega $P3\overline{m}1$ (a) $R\overline{3}m$ (b) structures with respect to the Cl-Cl distances between 3.5 and 4.0 Å. Still, also the hypothetical structure (c)-(f) exhibit peaks that coincide with those of the surface salt structure. Apparently, due to the lattice and symmetry mismatch between the hexagonally close-packed Mg(0001) surface within a 3×3 surface unit cell and the $MgCl_2$ bulk structure, no single $MgCl_2$ bulk structure can be deposited onto Mg(0001) in a commensurate pattern. Yet, by combining structural motifs of various possible $MgCl_2$ bulk structures, a rather stable $MgCl_2$-surface salt structure can be created. Similar structures might also be formed on other Mg structures including stepped and nanostructured surfaces [57] which optimize the interaction strength between the Mg substrate and the chloride surface salt.

CONCLUSIONS

In this theoretical work, we have determined the energetically stable chlorine adsorbate structures on Mg(0001) for nomimal chlorine coverages up to two monolayers. Such structures are relevant for the understanding of the conversion of the Mg anode in Cl-ion batteries upon discharge. Using a grand-canonical approach, we identified the thermodynamically stable Cl structures as a function of the applied electrode potential. Interestingly enough, it turns out that the layers with Cl atoms in the threefold hollow sites of Mg(0001) for a Cl coverage up to one monolayer are not thermodynamically stable. Instead, a three-dimensional surface salt structure with a nominal coverage of two chlorine monolayers identified by an adaptive random mutation hill climbing algorithm is the most stable structure. The comparison of the radial distribution function of this surface salt structure with those of various possible $MgCl_2$ bulk structure shows the adsorbate structure is based on a combination of possible $MgCl_2$ bulk structural motifs.

The thermodynamically stable direct formation of a $MgCl_2$ surface salt structure on Mg(0001) suggests that the conversion of the Mg anode to a $MgCl_2$ configuration upon discharge of a $MgCl_2$ batteries is directly initiated upon the exposure of the Mg anode to chloride ions. To the best of our knowledge, such a surface salt formation upon the exposure of a earth-alkaline metal to halides has not been identified before. Our work can thus serve as a crucial stepping stone towards unlocking the full potential of halide adsorption in next-generation electrochemical technologies, offering promising prospects for sustainable and energy-efficient energy storage solutions.

ACKNOWLEDGMENTS

Financial support by the Dr. Barbara Mez-Starck Foundation and by the German Research Foundation (DFG) under Project ID 390874152 (POLiS Cluster of Excellence, EXC 2154) is gratefully acknowledged. Computer time on the JUSTUS 2 cluster has been provided by the state of Baden-Württemberg through bwHPC and the German Research Foundation (DFG) through grant no INST 40/575-1 FUGG. This work contributes to the research performed at CELEST (Center for Electrochemical Energy Storage Ulm-Karlsruhe).

[1] O. M. Magnussen, Ordered anion adlayers on metal electrode surfaces, Chem. Rev. **107**, 679 (2002).

[2] F. Gossenberger, T. Roman, and A. Groß, Hydrogen and halide co-adsorption on Pt(111) in an electrochemical environment: a computational perspective, Electrochim. Acta **216**, 152 (2016).

[3] O. M. Magnussen and A. Groß, Toward an atomic-scale understanding of electrochemical interface structure and dynamics, J. Am. Chem. Soc. **141**, 4777 (2019).

[4] A. Groß, A. Eichler, J. Hafner, M. J. Mehl, and D. A. Papaconstantopoulos, Unified picture of the molecular adsorption process: O_2/Pt(111), Surf. Sci. **539**, L542 (2003).

[5] J. Yang, Y. Liu, Y. Zhang, G. Wang, X. Shi, H. Zhang, J. Li, P. Deng, and X. Tian, Recent advances and future perspectives of rechargeable chloride-based batteries, Nano Energy **110**, 108364 (2023).

[6] G. Karkera, M. A. Reddy, and M. Fichtner, Recent developments and future perspectives of anionic batteries, J. Power Sources **481**, 228877 (2021).

[7] X. Zhao, Z. Zhao-Karger, M. Fichtner, and X. Shen, Halide-based materials and chemistry for rechargeable batteries, Angew. Chem. Int. Ed. **59**, 5902 (2020).

[8] X. Zhao, Q. Li, Z. Zhao-Karger, P. Gao, K. Fink, X. Shen, and M. Fichtner, Magnesium anode for chloride ion batteries, ACS Appl. Mater. Interfaces **6**, 10997 (2014).

[9] Y. Tian, G. Zeng, A. Rutt, T. Shi, H. Kim, J. Wang, J. Koettgen, Y. Sun, B. Ouyang, T. Chen, Z. Lun, Z. Rong, K. Persson, and G. Ceder, Promises and challenges of next-generation "Beyond Li-ion´´ batteries for

electric vehicles and grid decarbonization, Chem. Rev. **121**, 1623 (2021).
[10] A. El Kharbachi, O. Zavorotynska, M. Latroche, F. Cuevas, V. Yartys, and M. Fichtner, Exploits, advances and challenges benefiting beyond Li-ion battery technologies, J. Alloys Compd. **817**, 153261 (2020).
[11] E. Bertel, K. Schwaha, and F. P. Netzer, Adsorption of bromine on Pt(111) - observation of an irreversible order-disorder transition, Surf. Sci. **83**, 439 (1979).
[12] W. Erley, Chlorine adsorption on the (111) faces of Pd and Pt, Surf. Sci. **94**, 281 (1980).
[13] A. Migani, C. Sousa, and F. Illas, Chemisorption of atomic chlorine on metal surfaces and the interpretation of the induced work function changes, Surf. Sci. **574**, 297 (2005).
[14] P. S. Bagus, C. Wöll, and A. Wieckowski, Dependence of surface properties on adsorbate-substrate distance: Work function changes and binding energy shifts for I/Pt(111), Surf. Sci. **603**, 273 (2009).
[15] T. Roman and A. Groß, Periodic density-functional calculations on work function change induced by adsorption of halogens on Cu(111), Phys. Rev. Lett. **110**, 156804 (2013).
[16] F. Gossenberger, T. Roman, K. Forster-Tonigold, and A. Groß, Change of the work function of platinum electrodes induced by halide adsorption, Beilstein J. Nanotechnol. **5**, 152 (2014).
[17] T. Roman, F. Gossenberger, K. Forster-Tonigold, and A. Groß, Halide adsorption on close-packed metal electrodes, Phys. Chem. Chem. Phys. **16**, 13630 (2014).
[18] P. Zhou, C. Zhou, and H. Gong, Chlorine adsorption on Mg, Ca, and MgCa surfaces, Mater. Sci. Eng. C **33**, 3826 (2013).
[19] Y.-H. Duan, Adsorption of fluorine and chlorine on Mg(0001) surface: A density functional theory investigation, Trans. Nonferrous Met. Soc. China **24**, 1844 (2014).
[20] Z. Luo, H. Zhu, T. Ying, D. Li, and X. Zeng, First principles calculations on the influence of solute elements and chlorine adsorption on the anodic corrosion behavior of Mg(0001) surface, Surf. Sci. **672-673**, 68 (2018).
[21] M. Todorova, E. Lundgren, V. Blum, A. Mikkelsen, S. Gray, J. Gustafson, M. Borg, J. Rogal, K. Reuter, J. Andersen, and M. Scheffler, The Pd(100)–(5×5)r27°–O surface oxide revisited, Surf. Sci. **541**, 101 (2003).
[22] E. Lundgren, A. Mikkelsen, J. N. Andersen, G. Kresse, M. Schmid, and P. Varga, Surface oxides on close-packed surfaces of late transition metals, J. Phys.: Condens. Matter **18**, R481 (2006).
[23] X. Lin, F. Gossenberger, and A. Groß, Ionic adsorbate structures on metal electrodes calculated from first-principles, Ind. Eng. Chem. Res. **55**, 11107 (2016).
[24] X. Lin, X. Tian, L. Song, M. Hua, and A. Groß, Restructuring of lead electrodes upon adsorption of NO_3^- anions studied from first-principles and its relevance for the operation of lead quantum switches, J. Phys. Chem. C **125**, 17962 (2021).
[25] F. Xie, R. Maul, C. Obermair, W. Wenzel, G. Schön, and T. Schimmel, Multilevel atomic-scale transistors based on metallic quantum point contacts, Adv. Mater. **22**, 2033 (2010).
[26] F.-Q. Xie, X.-H. Lin, A. Gross, F. Evers, F. Pauly, and T. Schimmel, Multiplicity of atomic reconfigurations in an electrochemical Pb single-atom transistor, Phys. Rev. B **95**, 195415 (2017).
[27] M. Jäckle, K. Helmbrecht, M. Smits, D. Stottmeister, and A. Groß, Self-diffusion barriers: Possible descriptors for dendrite growth in batteries?, Energy Environ. Sci. **11**, 3400 (2018).
[28] K. Reuter and M. Scheffler, Composition, structure, and stability of RuO_2(110) as a function of oxygen pressure, Phys. Rev. B **65**, 035406 (2001).
[29] A. A. Peterson, F. Abild-Pedersen, F. Studt, J. Rossmeisl, and J. K. Nørskov, How copper catalyzes the electroreduction of carbon dioxide into hydrocarbon fuels, Energy Environ. Sci. **3**, 1311 (2010).
[30] A. Groß, Grand-canonical approaches to understand structures and processes at electrochemical interfaces from an atomistic perspective, Curr. Opin. Electrochem. **27**, 100684 (2021).
[31] A. Groß, Reversible vs standard hydrogen electrode scale in interfacial electrochemistry from a theoretician's atomistic point of view, J. Phys. Chem. C **126**, 11439 (2022).
[32] G. Kresse and J. Furthmüller, Efficient iterative schemes for ab initio total-energy calculations using a plane-wave basis set, Phys. Rev. B **54**, 11169 (1996).
[33] G. Kresse and J. Furthmüller, Comput. Mater. Sci. **6**, 15 (1996).
[34] H. Euchner and A. Groß, Atomistic modeling of li- and post-li-ion batteries, Phys. Rev. Mater. **6**, 040302 (2022).
[35] J. P. Perdew, K. Burke, and M. Ernzerhof, Phys. Rev. Lett. **77**, 3865 (1996).
[36] M. Jäckle and A. Groß, Influence of electric fields on metal self-diffusion barriers and its consequences on dendrite growth in batteries, J. Chem. Phys. **151**, 234707 (2019).
[37] P. E. Blöchl, Projector augmented-wave method, Phys. Rev. B **50**, 17953 (1994).
[38] G. Kresse and D. Joubert, From ultrasoft pseudopotentials to the projector augmented-wave method, Phys. Rev. B **59**, 1758 (1999).
[39] C. Kittel, *Introduction to solid state physics* (John Wiley & sons, inc, 2005).
[40] G. Walker and M. Marezio, Lattice parameters and zone overlap in solid solutions of lead in magnesium, Acta Metall. **7**, 769 (1959).
[41] E. R. Jette and F. Foote, Precision determination of lattice constants, J. Chem. Phys. **3**, 605 (2004).
[42] H. A. Hansen, I. C. Man, F. Studt, F. Abild-Pedersen, T. Bligaard, and J. Rossmeisl, Electrochemical chlorine evolution at rutile oxide (110) surfaces, Phys. Chem. Chem. Phys. **12**, 283 (2010).
[43] F. Gossenberger, T. Roman, and A. Groß, Equilibrium coverage of halides on metal electrodes, Surf. Sci. **631**, 17 (2015).
[44] M. Lischka, C. Mosch, and A. Groß, Tuning catalytic properties of bimetallic surfaces: Oxygen adsorption on pseudomorphic Pt/Ru overlayers, Electrochim. Acta **52**, 2219 (2007).
[45] A. Groß, *Theoretical surface science – A microscopic perspective*, 2nd ed. (Springer, Berlin, 2009).

[46] J. L. Da Silva, C. Stampfl, and M. Scheffler, Converged properties of clean metal surfaces by all-electron first-principles calculations, Surf. Sci. **600**, 703 (2006).
[47] P. Sprunger, K. Pohl, H. Davis, and E. Plummer, Multilayer relaxation of the mg(0001) surface, Surf. Sci. **297**, L48 (1993).
[48] Ismail, P. Hofmann, A. P. Baddorf, and E. W. Plummer, Thermal expansion at a metal surface: A study of Mg(0001) and Be(101$\bar{0}$), Phys. Rev. B **66**, 245414 (2002).
[49] Y. Li, P. Zhang, B. Sun, Y. Yang, and Y. Wei, Atomic hydrogen adsorption and incipient hydrogenation of the mg(0001) surface: A density-functional theory study, J. Chem. Phys. **131**, 034706 (2009).
[50] K. Sarkar and S. P. Bhattacharyya, Single string based global optimizer for geometry optimization in strongly coupled finite clusters: An adaptive mutation-driven strategy, J. Chem. Phys. **139**, 074106 (2013).
[51] K. Sarkar and S. P. Bhattacharyya, *Soft computing in chemical and physical sciences: a shift in computing paradigm* (CRC Press, 2017).
[52] K. Sarkar, N. Holzwarth, and R. Wentzcovitch, Epaw-1.0 code for evolutionary optimization of paw datasets especially for high-pressure applications, Comp. Phys. Comm. **233**, 110 (2018).
[53] I. W. Bassi, F. Polato, M. Calcaterra, and J. C. J. Bart, A new layer structure of mgcl2 with hexagonal close packing of the chlorine atoms, Z. Kristallographie - Crystal. Mater. **159**, 297 (1982).
[54] D. Partin and M. O'Keeffe, The structures and crystal chemistry of magnesium chloride and cadmium chloride, Journal of Solid State Chemistry **95**, 176 (1991).
[55] A. Jain, S. P. Ong, G. Hautier, W. Chen, W. D. Richards, S. Dacek, S. Cholia, D. Gunter, D. Skinner, G. Ceder, and K. A. Persson, Commentary: The Materials Project: A materials genome approach to accelerating materials innovation, APL Materials **1**, 011002 (2013).
[56] M. W. Terban and S. J. L. Billinge, Structural analysis of molecular materials using the pair distribution function, Chem. Rev. **122**, 1208 (2022).
[57] A. Groß, Adsorption at nanostructured surfaces from first principles, J. Comput. Theor. Nanosci. **5**, 894 (2008).